GaInN light-emitting diode with conductive omnidirectional reflector having a low-refractive-index indium-tin oxide layer

Jong Kyu Kim, Thomas Gessmann, and E. Fred Schubert[a)]
Department of Electrical, Computer, and Systems Engineering, Rensselaer Polytechnic Institute, Troy, New York 12180

J.-Q. Xi and Hong Luo
Department of Physics, Applied Physics, and Astronomy, Rensselaer Polytechnic Institute, Troy, New York 12180

Jaehee Cho, Cheolsoo Sone, and Yongjo Park
Photonics Program Team, Samsung Advanced Institute of Technology, Suwon 440-600, South Korea

(Received 31 August 2005; accepted 28 November 2005; published online 3 January 2006)

Enhancement of light extraction in a GaInN light-emitting diode (LED) employing a conductive omnidirectional reflector (ODR) consisting of GaN, an indium-tin oxide (ITO) nanorod low-refractive-index layer, and an Ag layer is presented. An array of ITO nanorods is deposited on *p*-type GaN by oblique-angle electron-beam deposition. The refractive index of the nanorod ITO layer is 1.34 at 461 nm, significantly lower than that of dense ITO layer, which is $n=2.06$. The GaInN LEDs with GaN/low-n ITO/Ag ODR show a lower forward voltage and a 31.6% higher light-extraction efficiency than LEDs with Ag reflector. This is attributed to enhanced reflectivity of the ODR that employs the low-n ITO layer. © *2006 American Institute of Physics*.
[DOI: 10.1063/1.2159097]

GaN-based light-emitting diodes (LEDs) provide a higher performance in the ultraviolet and short-wavelength part of the visible spectrum than any other material system. However, there is still a great need for improvement of the light-extraction efficiency, as well as the internal quantum efficiency. There are several ways to obtain high extraction efficiency including shaping of LED dies,[1] flip-chip mounting,[2] roughening of the top LED surface,[3] and introducing highly reflective triple-layer omnidirectional reflectors (ODRs).[4,5] Recently, LEDs with triple-layer ODRs have been demonstrated to have a wide stop band, omnidirectional reflection characteristics, and higher reflectivity than conventional distributed Bragg reflectors (DBRs) and Ag reflectors. The ODRs (Refs. 4 and 5) consisted of a semiconductor (GaN), a quarter-wavelength-thick SiO_2 low-refractive-index (low-n) layer perforated by an array of microcontacts enabling electrical conductivity through the insulating SiO_2 layer, and an Ag layer.

The triple-layer ODR can be considered as a degenerate hybrid DBR/metal reflector. For DBRs, the reflectivity and spectral width of the high-reflectivity stop band directly depend on the refractive index contrast, i.e., the difference in refractive index between the high-index and low-index material. The higher the refractive index contrast, the higher the reflectivity, and the wider the spectral width of the stop band. Reducing the refractive index of the low-refractive-index layer, and hence increasing the refractive index contrast, would further improve the reflectivity of GaN-based ODRs.[6] This motivates the development of new optical thin-film materials with low-refractive index, high transparency, and high conductivity.

In this work, a conductive ODR consisting of GaN, Ag, and an intermediate indium-tin oxide (ITO) nanorod low-n layer is incorporated into a GaInN LED. An array of ITO nanorods is deposited by oblique-angle electron-beam (e-beam) deposition. It is found that the refractive index of a *nanorod* ITO layer at 461 nm is only 1.34, significantly lower than that of a *dense* ITO layer, which is $n=2.06$. It is shown that GaInN LEDs with GaN/low-n ITO/Ag ODRs have excellent electrical and optical properties.

Oblique-angle deposition is a method to grow thin films with a porous microstructure, caused by the self-shadowing nature of the deposition process.[6–9] Figure 1(a) shows the principle of oblique-angle deposition. A random growth fluctuation on the substrate produces a *shadow region* that the incident vapor flux cannot reach, and a *nonshadow region*

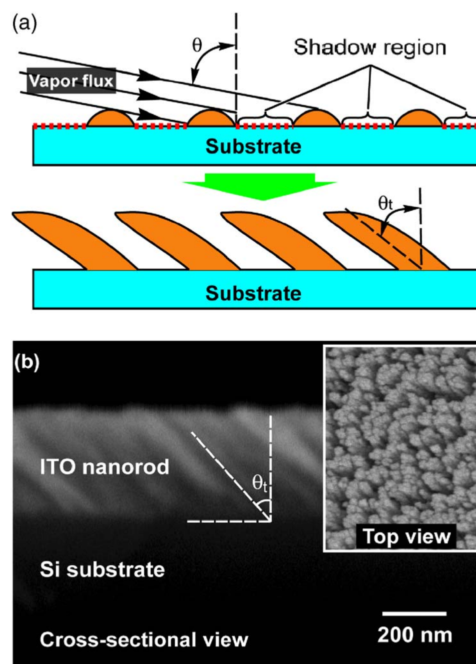

FIG. 1. (a) Schematic of oblique-angle deposition. (b) Scanning electron micrograph showing an array of ITO nanorods deposited by oblique-angle e-beam evaporation on a Si substrate.

[a)]Electronic mail: efschubert@rpi.edu

 © 2006 American Institute of Physics
Downloaded 03 Jan 2006 to 128.113.123.170. Redistribution subject to AIP license or copyright, see http://apl.aip.org/apl/copyright.jsp

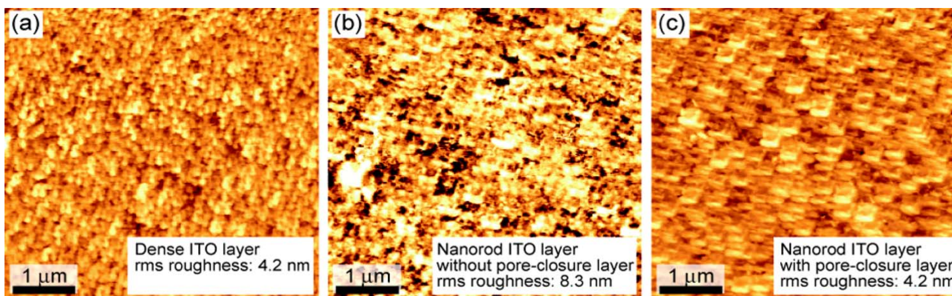

FIG. 2. AFM images of the surface of (a) dense ITO layer and nanorod ITO layer (b) without and (c) with pore-closure layer.

where incident flux deposits preferentially, thereby creating an oriented rodlike structure. In order to grow highly porous thin films, the incidence angle of the vapor flux, θ, must be large. Several ITO test films, grown by oblique-angle e-beam deposition on Si substrates with a vapor flux incident angle θ of 80°, are found to be optically transparent and electrically conductive. Pure ITO granules are used as the evaporation source, and the deposition rate is well controlled at 5 Å/s. Figure 1(b) shows the cross-sectional scanning electron micrograph (SEM) of the nanorod ITO layer. The nanorod ITO is uniformly distributed with tilt angle of $\theta_t=45°$. The gap between the nanorod ITO is less than 50 nm, i.e., much smaller than the wavelength of visible light, thereby limiting optical scattering. The nanorod ITO thin film obtained by the oblique-angle deposition is specular, featureless, and virtually colorless and transparent. Furthermore, since the film is deposited by evaporation, the controllability of film thickness is excellent, very suitable for quarter-wavelength optical films. Therefore, oblique-angle deposition is promising for the growth of optical coatings with very low-refractive index, which are advantageous for high-refractive-index contrast ODRs.

The inset in Fig. 1(b) shows the SEM top view of the nanorod ITO film including openings between the nanorods. In order to avoid the filling of subsequent metal into these openings, a surface-sealing step is employed by depositing a pore-closure layer. The deposition conditions of the pore-closure layer are the same as that for the nanorod ITO layer except that the vapor flux incidence angle is $\theta=-45°$. The nanorod orientation of the pore-closure layer is thus near perpendicular to the orientation of the main film, thereby reducing the ability of the metal to be deposited on top of the nanorod film to enter the openings between the nanorods.

The atomic-force microscopy (AFM) images of the surface of dense ITO layer and the nanorod ITO layer with and without a pore-closure layer are shown in Fig. 2. The root-mean-square (rms) surface roughness of the dense ITO layer, which is e-beam deposited with normal incidence of the vapor flux, is 4.2 nm. The rms roughness of the nanorod ITO layer without a pore-closure layer is 8.3 nm, higher than that of the dense ITO layer, due to the openings between the nanorods. After the pore-closure layer deposition, the rms roughness reduces to 4.2 nm, and there is no indication of openings between the nanorods. This shows that the deposition of the pore-closure layer reduces openings thereby making the nanorod ITO films suitable for advanced multilayers structures.

The refractive index of the nanorod ITO films is measured with ellipsometry using the incident angles 60°, 65°, and 70°. A "Cauchy layer on Si substrate" is used as the ellipsometry model and found to fit the measurement data very well. The refractive index of the nanorod ITO films versus wavelength is shown in Fig. 3. Over the entire visible spectrum, the refractive index of the nanorod ITO layer is $n<1.35$. The refractive index at 461 nm of the nanorod ITO layer is $n=1.34$, much lower than the refractive index of dense ITO layer, $n=2.06$, and even lower than that of SiO_2, $n=1.46$. The thickness of the nanorod ITO layer determined from the ellipsometry measurement is $h=334$ nm, confirming the thickness obtained from the SEM image shown in Fig. 1(b). The nanorod ITO layer is shown to have a very low-refractive layer and we henceforth call this layer "low-n ITO" layer.

The refractive index of a porous material is determined by the porosity and refractive index of the dense material. For two components with volume fractions V_{Air} and V_{ITO}, where $V_{\mathrm{Air}}+V_{\mathrm{ITO}}=1.0$, and refractive indices n_{Air} and n_{ITO}, the Bruggemann effective medium approximation gives[10]

$$V_{\mathrm{Air}}\frac{n_{\mathrm{Air}}^2-n_{\mathrm{eff}}^2}{n_{\mathrm{Air}}^2+2n_{\mathrm{eff}}^2}+(1-V_{\mathrm{Air}})\frac{n_{\mathrm{ITO}}^2-n_{\mathrm{eff}}^2}{n_{\mathrm{ITO}}^2+2n_{\mathrm{eff}}^2}=0,$$

where n_{eff} is effective refractive index and V_{Air} is volume fraction of air (or porosity of film). The porosity V_{Air} of the low-n ITO layer is calculated to be 64.3% using parameters, $n_{\mathrm{eff}}=1.34$, $n_{\mathrm{ITO}}=2.06$, and $n_{\mathrm{Air}}=1.0$.

The low-n ITO is incorporated into a GaInN LED emitting at a peak wavelength of 474 nm. The GaInN LED structure was grown by metalorganic chemical vapor deposition on a c-plane sapphire substrate and consists of a 3-μm-thick n-type GaN buffer layer, an n-type GaN lower cladding layer, a GaInN/GaN multiple quantum-well active region, a p-type GaN upper cladding layer, and a highly doped p-type GaN contact layer. A quarter-wavelength-thick low-n ITO layer was deposited by oblique-angle e-beam deposition with

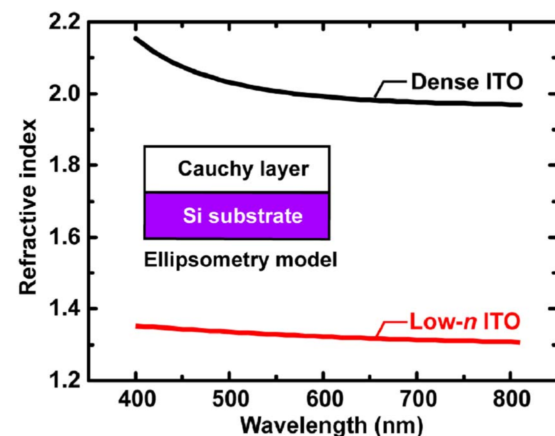

FIG. 3. Refractive index of dense ITO and low-n ITO films vs wavelength measured using ellipsometry. The samples are measured at incident angles 60°, 65°, and 70°. The ellipsometry model is a Cauchy layer on Si substrate.

Downloaded 03 Jan 2006 to 128.113.123.170. Redistribution subject to AIP license or copyright, see http://apl.aip.org/apl/copyright.jsp

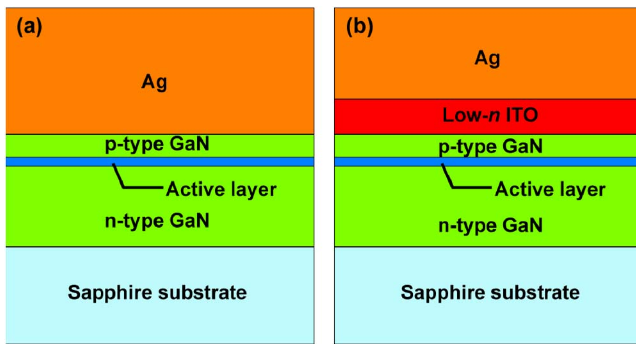

FIG. 4. Schematic cross-sectional view of GaInN LED with (a) Ag reflector and (b) GaN/low-*n* ITO/Ag ODR.

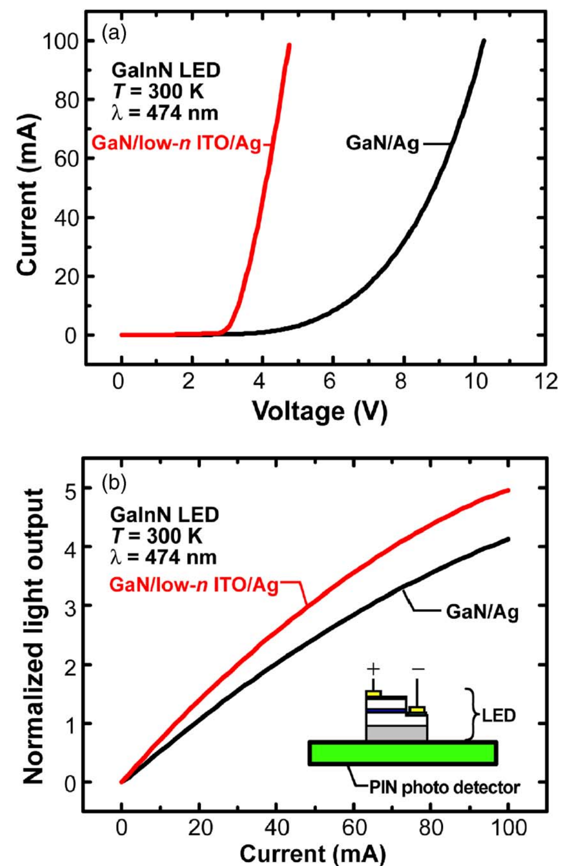

FIG. 5. (a) Current-voltage characteristics and (b) light-output-versus-current characteristic of typical GaInN LED with GaN/low-*n* ITO/Ag ODR and of typical LED with Ag reflector.

an incident angle of 80°. After the low-*n* ITO deposition, a very thin (20 nm) pore-closure layer is formed on top of the low-*n* ITO layer with an incident angle of −45°. After the pore-closure layer, a 200-nm-thick Ag layer is deposited by e-beam evaporation. LED mesa structures were obtained by standard photolithographic patterning followed by chemically assisted ion-beam etching using Cl_2 and Ar, to expose the *n*-type cladding layer. For comparison, LEDs with a Ag reflector were fabricated on the same wafer piece. Figures 4(a) and 4(b) show schematic cross-sectional views of the GaInN LED with an Ag reflector and the ODR with low-*n* ITO layer, respectively. The *n*-type contact for all samples is e-beam evaporated Ti/Al/Ni/Au annealed at 650 °C for 1 min.

Figure 5(a) shows typical current-voltage characteristics of the LEDs with GaN/low-*n* ITO/Ag ODR and of the LEDs with Ag reflector. The forward voltage at 20 mA for the GaN/low-*n* ITO/Ag ODR LEDs is 3.5 V, much lower than that for the LEDs with the Ag reflector. The electroluminescence intensity from the back side of the LED was measured directly on a large-size (10×10 mm^2) Si *p*-*i*-*n* photodetector. A typical light-output-versus-current characteristics of the LEDs is shown in Fig. 5(b). The light-output power of the GaN/low-*n* ITO/Ag ODR LEDs is significantly higher than that of the LEDs with the Ag reflector. At an injection current of 20 mA, the enhancement in light output of the LEDs with GaN/low-*n* ITO/Ag ODR is 31.6%, compared to the LEDs with the Ag reflector. The increased light output of the LEDs with GaN/low-*n* ITO/Ag ODR is attributed to higher reflectivity and lower losses of waveguided optical modes. The better light-extraction efficiency is due to the high-refractive-index contrast enabled by the low-*n* ITO layer.

In summary, we presented enhanced light output in GaInN blue LEDs by employing an ODR with a low-*n* ITO layer fabricated by oblique-angle e-beam deposition. The low-*n* ITO layer exhibits high transparency, high conductivity, and low-refractive index. The refractive index of the low-*n* ITO layer is 1.34 at 461 nm, significantly lower that that of dense ITO layer, $n=2.06$. Current-voltage characteristics show that a forward voltage of the GaN/low-*n* ITO/Ag ODR LEDs is 3.5 V, much lower than that of the LEDs with the Ag reflector. Furthermore, the light output of the GaN/low-*n* ITO/Ag ODR LEDs is much higher than that of the LEDs with the Ag reflector. Compared to the LEDs with the Ag reflector, the improvement of light output of the GaN/low-*n* ITO/Ag ODR LEDs is 31.6% at an injection current of 20 mA. The improvement is attributed to enhanced reflectivity of the ODR and lower losses of waveguided modes.

The authors gratefully acknowledge support from National Science Foundation (NSF), the Defense Advanced Research Projects Agency (DARPA), the Army Research Office (ARO), Samsung Advanced Institute of Technology (SAIT), and Crystal IS Corporation.

[1]M. R. Krames, M. Ochiai-Holcomb, G. E. Höfler, C. Carter-Coman, E. I. Chen, M. G. Craford, T. S. Tan, C. P. Kocot, M. Hueschen, J. Posselt, B. Loh, G. Sasser, and D. Collins, Appl. Phys. Lett. **75**, 2365 (1999).
[2]J. J. Wierer, D. A. Steigerwald, M. R. Krames, J. J. O'Shea, M. J. Ludowise, G. Christenson, Y.-C. Shen, C. Lowery, P. S. Martin, S. Subramanya, W. Götz, N. F. Gardner, R. S. Kern, and S. A. Stockman, Appl. Phys. Lett. **78**, 3379 (2001).
[3]T. Fujii, Y. Gao, R. Sharma, E. L. Hu, S. P. DenBaars, and S. Nakamura, Appl. Phys. Lett. **84**, 855 (2004).
[4]T. Gessmann, E. F. Schubert, J. W. Graff, K. Streubel, and C. K. Arnutsch, IEEE Electron Device Lett. **24**, 683 (2003).
[5]J. K. Kim, T. Gessmann, H. Luo, and E. F. Schubert, Appl. Phys. Lett. **84**, 4508 (2004).
[6]J.-Q. Xi, J. K. Kim, and E. F. Schubert, Nano Lett. **5**, 1385 (2005).
[7]K. Robbie, L. J. Friedrich, S. K. Dew, T. Smy, and M. J. Brett, J. Vac. Sci. Technol. A **13**, 1032 (1995).
[8]D. Vick, J. J. Friedrich, S. K. Dew, M. J. Brett, K. Robbie, M. Seto, and T. Smy, Thin Solid Films **339**, 88 (1999).
[9]K. Kaminska and K. Robbie, Appl. Opt. **43**, 1570 (2004).
[10]K. H. H. Peter, T. D. Stephen, H. F. Richard, and T. Nir, Science **285**, 233 (1999).

Downloaded 03 Jan 2006 to 128.113.123.170. Redistribution subject to AIP license or copyright, see http://apl.aip.org/apl/copyright.jsp